Dynamic analysis of a seismically induced mass movement after the December 2018 Etna volcano eruption

M. Albano[1], M. Saroli[2,1], S. Atzori[1], M. Moro[1], C. Tolomei[1], C. Bignami[1], S. Stramondo[1]

[1]Istituto Nazionale di Geofisica e Vulcanologia, Roma, Italy.

[2]Dipartimento di Ingegneria Civile e Meccanica (DICeM), Università degli Studi di Cassino e del Lazio meridionale, Cassino (FR), Italy.

Introduction. On December 24, 2018, Etna volcano began a very intense eruption, featuring massive ash and gas emissions, lava flows, and a seismic swarm with magnitudes less than 5. Hundreds of earthquakes (Fig. 1) were associated with a dyke intrusion in the upper part of the Etna volcano, which induced significant deformation of the volcanic edifice (Bonforte et al., 2019; De Novellis et al., 2019). The dyke intrusion encouraged, with favourable stress loading, seismic dislocation of the Fiandaca Fault (Fig. 1) (De Novellis et al., 2019). A strike-slip earthquake (M_w 4.9) nucleated on December 26, 2018, at a focal depth of approximately 1 km, causing ground fractures and seismic shaking with PGA up to 0.075g, which caused some damage to nearby villages (Villani et al., 2020).

Space-borne synthetic aperture radar (SAR) data from Sentinel-1 (hereinafter S-1) provided a stunning picture of the displacement fields caused by volcanic eruption and earthquake dislocation (Bignami et al., 2019; Bonforte et al., 2019; De Novellis et al., 2019). Fig. 1a shows the wrapped displacement observed in the period December 22-28, 2018 along the descending line of sight (LoS), that is the direction of the shortest path between a point on the Earth's surface and the SAR antenna. One highly visible deformation pattern is located along Mt. Etna's flanks, where a bi-lobate interferometric fringe pattern highlights the deformation induced by dyke intrusion (Bonforte et al., 2019; De Novellis et al., 2019). A second deformation pattern is localised to the S-E of Etna volcano, where small fringe pattern identifies the displacements caused by the December 26, M_w 4.9 strike-slip dislocation of the Fiandaca Fault (De Novellis et al., 2019). Local small interferometric fringes identify a third deformation pattern over a hilly area located approximately 5 km west of Paternò village (the dashed black box in Fig. 1a) (Bignami et al., 2019). This displacement is not related to volcanic inflation or fault dislocation, because no large earthquakes have occurred nearby. The unwrapped S-1 interferograms (Fig. 1b) show that displacements reach approximately 6 cm at the foot of the hill along both the descending and ascending orbits and gradually vanish towards the boundaries of the DGSD. The similarity of displacement amplitudes and spatial extents along satellite trajectories with different signs (negative and positive displacements indicate movements away from and towards the satellite sensor, respectively) suggest that horizontal displacements dominate the actual movement. Bignami et al. (2019) interpreted this displacement as potentially associated with the seismic reactivation of a paleo-landslide.

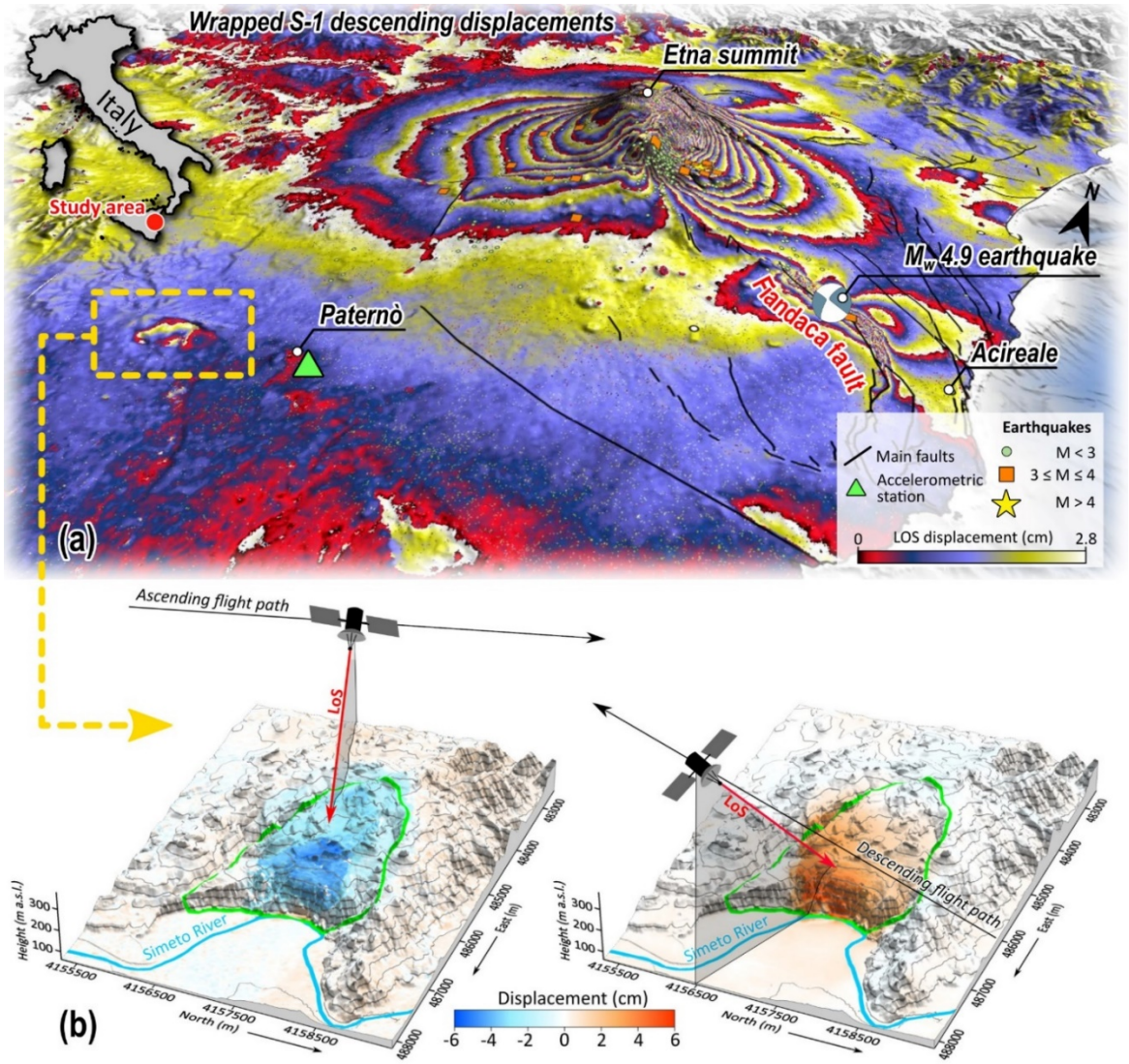

Fig.1 - (a) Sketch of the Etna volcano area. The coloured pattern identifies wrapped ground displacements from the Sentinel-1 descending interferogram (22/12/2018 – 28/12/2018), and highlights the deformations caused by the Mt Etna volcanic inflation, the December 26 M_w 4.9 earthquake along the Fiandaca Fault, and the mass movement to the west of Paternò village. (b) LoS displacement pattern along the ascending (left) and descending (right) orbits given by the processing of the S-1 data in the time interval of December 22 – 28, 2018.

Data and methods. To unveil the phenomenon that caused the observed displacements, the interplay between the ground movements and seismic shaking produced by the M_w 4.9 event has been investigated thorough a multidisciplinary analysis comprising seismological, geological and geomorphological data, together with analytical and dynamic models. A permanent displacement approach (Newmark, 1965) has been applied to investigate the seismic behaviour of the slope (Albano et al., 2018; Di Naccio et al., 2019). To this aim, we performed a back-analysis of the observed sliding mass movements.

Back-analysing slope movements involves determining the shear strength of the soil mass, given the conditions that existed at the time of failure, such as the pore-water pressure distribution, the characteristics of the seismic load, and the geometry and slip of the sliding surface. The latter could be unknown in the case of non-catastrophic slope movement involving blind surfaces, as in this case study. To estimate the required parameters, we followed these steps:

i) Estimation of the geometry and slip distribution of the potential sliding surface by analytical inversion of the observed InSAR displacement, assuming a planar source embedded in an elastic medium;

ii) Assessment of the critical soil strength parameters by performing a pseudostatic limit equilibrium analysis of the slope, considering the slip of the sliding surface, the seismic input and the critical acceleration (a_c) of the slope;

iii) Validation of the computed strength parameters by comparison with those provided by laboratory and in situ surveys.

Results. Geological and geomorphological analyses identified several features in the area, such as double crest lines, scarps, counterscarps, trenches, and depression alignments, which are typical indicators of the presence of active or quiescent mass movements. Two unknown Deep-seated Gravitational Slope Deformations (DGSD) were identified (Fig. 2a) whose kinematics are governed by deep sliding surfaces, beginning at the top of the DGSD bodies and ending at the toe of the hill to the E, close to the Simeto River (the dashed red curves in Fig. 2a). The potential sliding surfaces are sub-planar, with a gentle slope, and involve a potential soil mass volume of approximately 3 - 4 x 10^8 m^3 with a mean thickness of approximately 100-150 m. The likely detachment is hypothesised to be at the interface between brown brecciated clays (3a in Fig. 2a) and grey-blue and brown marly clays (3b in Fig. 2a).

The inversion of InSAR displacements identified a slip plane (Fig. 2b) located below the DGSD at an average height of approximately 90 m a.s.l., with a length of 1450 m, a width of 1750 m, a dip of approximately 2.3° towards E, and a slip distribution peaking at 8.5 cm and directed towards the E (i.e., rake ≈ 100°). Such a sliding plane is compatible with the potential sliding surface identified from geomorphological analyses (Fig. 2a). Finally, we estimated the critical soil strength parameters by performing a pseudostatic limit equilibrium analysis assuming an infinite slope scheme and considering both drained and undrained conditions for the soil behaviour. We assumed as seismic input the E-W component of the acceleration time history associated to the December 26, 2018 M_w 4.9 earthquake, registered at the PTR station (Fig. 1a), with this component being the most energetic (PGA ≈ 0.01g) and perfectly aligned with the DGSD sliding plane orientation and slip direction.

For drained conditions, the critical friction angle (ϕ_c) ranges between 2.4 and 2.8 degrees, with a median value of approximately 2.5. These values are not compatible with the experimental distribution of ϕ, ranging between 18 and 27 degrees. For undrained conditions, the critical undrained cohesion ($c_{u,c}$) ranges between 30 and 200 kPa, with a median value of approximately 132 kPa. Such values are consistent with the experimental distribution of c_u shown in Fig. 2c.

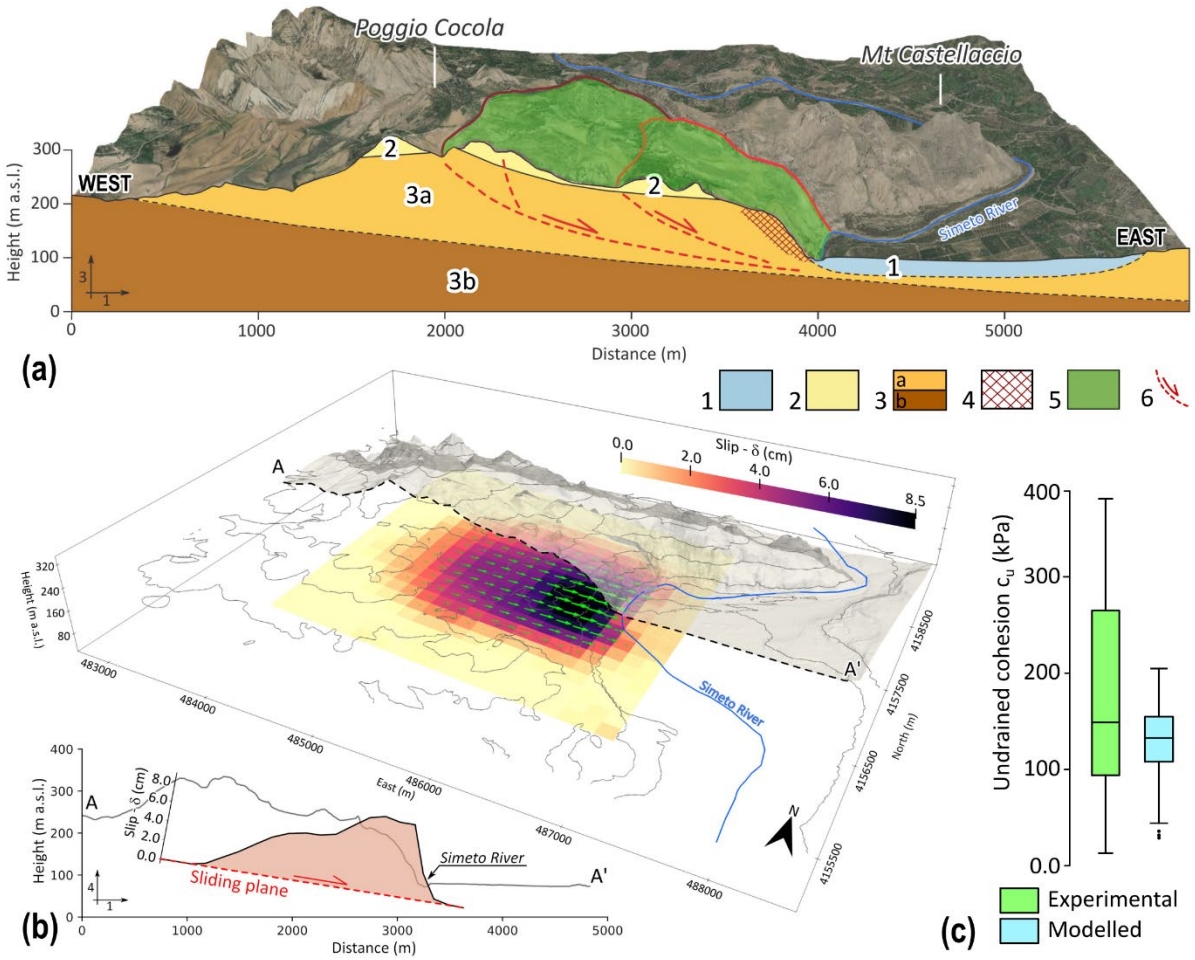

Fig.2 - (a) Geological cross-section of the DGSD. Key to the legend: 1. Recent and old terraced alluvial deposits (Holocene); 2. Marly limestone and limestone breccias with gypsum (Messinian-lower Pliocene); 3a, b. Terravecchia formation (upper Tortonian); 4. Areas affected by surficial landslides; 5. DGSD body; 6. Inferred DGSD sliding surface. (b) 3D geometry and slip distribution of the potential sliding plane responsible for the observed ground displacements. (c) Comparison between experimental and modelled undrained cohesion (c_u).

Conclusions. The interplay between volcano-tectonic earthquakes and the triggering of non-catastrophic landslide movement has been investigated by applying a multidisciplinary approach. Geological and geomorphological analyses provided evidence of a previously unknown paleo-landslide located 5 km west of Paternò village with an overall extent of approximately 3.40 km^2. InSAR data show that the landslide mass, which was in a dormant phase, was reactivated during the Etna volcano eruption and the related seismic swarm. Analytical inversion of InSAR data identified the geometry and kinematics of the potential sliding surface, whose geometry and position are in accordance with geological and geomorphological findings. The back-analysis of the observed ground displacements confirmed that the landslide mass reactivated during the light-to-moderate seismic shaking caused by the December 26 M_w 4.9 earthquake 25 km away. The earthquake caused undrained instability of the landslide and ground displacement.

References

Albano, M., Saroli, M., Montuori, A., Bignami, C., Tolomei, C., Polcari, M., Pezzo, G., Moro, M., Atzori, S., Stramondo, S., Salvi, S.; 2018: *The Relationship between InSAR Coseismic Deformation and Earthquake-Induced Landslides Associated with the 2017 Mw 3.9 Ischia (Italy) Earthquake*. Geosciences **8**, 303. https://doi.org/10.3390/geosciences8080303

Bignami, C., Salvi, S., Albano, M., Guglielmino, F., Tolomei, C., Atzori, S., Trasatti, E., Polcari, M., Puglisi, G., Stramondo, S.;2019: *Multi-Hazard Analysis of Etna 2018 Eruption by Sar Imaging*, in: IGARSS 2019 - 2019 IEEE International Geoscience and Remote Sensing Symposium. IEEE, pp. 9314–9317. https://doi.org/10.1109/IGARSS.2019.8898695

Bonforte, A., Guglielmino, F., Puglisi, G.; 2019: *Large dyke intrusion and small eruption: The December 24, 2018 Mt. Etna eruption imaged by Sentinel-1 data*. Terra Nova **31**, 405–412. https://doi.org/10.1111/ter.12403

De Novellis, V., Atzori, S., De Luca, C., Manzo, M., Valerio, E., Bonano, M., Cardaci, C., Castaldo, R., Di Bucci, D., Manunta, M., Onorato, G., Pepe, S., Solaro, G., Tizzani, P., Zinno, I., Neri, M., Lanari, R., Casu, F.; 2019: *DInSAR Analysis and Analytical Modeling of Mount Etna Displacements: The December 2018 Volcano-Tectonic Crisis*. Geophys. Res. Lett. **46**, 5817–5827. https://doi.org/10.1029/2019GL082467

Di Naccio, D., Kastelic, V., Carafa, M.M.C., Esposito, C., Milillo, P., Di Lorenzo, C.; 2019: *Gravity Versus Tectonics: The Case of 2016 Amatrice and Norcia (Central Italy) Earthquakes Surface Coseismic Fractures*. J. Geophys. Res. Earth Surf. **124**, 994–1017. https://doi.org/10.1029/2018JF004762

Newmark, N.M.; 1965: *Effects of Earthquakes on Dams and Embankments*. Géotechnique **15**, 139–160. https://doi.org/10.1680/geot.1965.15.2.139

Villani, F., Pucci, S., Azzaro, R., Civico, R., Cinti, F.R., Pizzimenti, L., Tarabusi, G., Branca, S., Brunori, C.A., Caciagli, M., Cantarero, M., Cucci, L., D'Amico, S., De Beni, E., De Martini, P.M., Mariucci, M.T., Messina, A., Montone, P., Nappi, R., Nave, R., Pantosti, D., Ricci, T., Sapia, V., Smedile, A., Vallone, R., Venuti, A.; 2020: *Surface ruptures database related to the 26 December 2018, MW 4.9 Mt. Etna earthquake, southern Italy*. Sci. Data **7**, 42. https://doi.org/10.1038/s41597-020-0383-0

Corresponding author: matteo.albano@ingv.it